J. Fluid Mech. (2010), *vol.* 657, *pp.* 171–188. © Cambridge University Press 2010
doi:10.1017/S0022112010001400

The bottleneck effect and the Kolmogorov constant in isotropic turbulence

D. A. DONZIS[1]† AND K. R. SREENIVASAN[2,3]

[1]Department of Aerospace Engineering, Texas A&M University, College Station, TX 77843, USA

[2]Institute for Physical Science and Technology, University of Maryland, College Park, MD 20742, USA

[3]Department of Physics and the Courant Institute of Mathematical Sciences, New York University, New York, NY 10012, USA

(Received 17 August 2009; revised 15 March 2010; accepted 15 March 2010; first published online 10 June 2010)

A large database from direct numerical simulations of isotropic turbulence, including recent simulations for box sizes up to 4096^3 and the Taylor–Reynolds number $R_\lambda \approx 1000$, is used to investigate the bottleneck effect in the three-dimensional energy spectrum and second-order structure functions, and to determine the Kolmogorov constant, C_K. The difficulties in estimating C_K at any finite Reynolds number, introduced by intermittency and the bottleneck, are assessed. The data conclusively show that the bottleneck effect decreases with the Reynolds number. On this basis, an alternative to the usual procedure for determining C_K is suggested; this proposal does not depend on the particular choices of fitting ranges or power-law behaviour in the inertial range. Within the resolution of the numerical data, C_K thus determined is a Reynolds-number-independent constant of ≈ 1.58 in the three-dimensional spectrum. A simple model including non-local transfer is proposed to reproduce the observed scaling features of the bottleneck.

1. Introduction

The classical phenomenology of Kolmogorov (1941) bestows a certain universality on small scales of turbulent motion at large Reynolds numbers. Specifically, the three-dimensional energy spectrum $E(k)$, for wavenumbers $kL \gg 1$, where L is the scale at which turbulent energy is injected, is given by

$$\frac{E(k)}{u_\eta^2 \eta} = F(k\eta). \tag{1.1}$$

Here, $\eta = (\nu^3/\langle\epsilon\rangle)^{1/4}$ and $u_\eta = (\nu\langle\epsilon\rangle)^{1/4}$ are the Kolmogorov length and velocity scales, respectively, ν is the viscosity and $\langle\epsilon\rangle$ is the mean energy dissipation rate. In particular, the function $F(k\eta)$ is independent of how turbulence is created. It is also well known that the Kolmogorov–Obukhov arguments (Kolmogorov 1941; Obukhov 1941) yield $E(k) \sim k^{-5/3}$ in the inertial range given by $1/L \ll k \ll 1/\eta$. It is thus useful to rewrite (1.1) as

$$E(k) = C_K \langle\epsilon\rangle^{2/3} k^{-5/3} f(k\eta), \tag{1.2}$$

where $f(k\eta)$ is a universal function with the property $f(0) = 1$ and C_K is the Kolmogorov constant.

† Email address for correspondence: donzis@tamu.edu

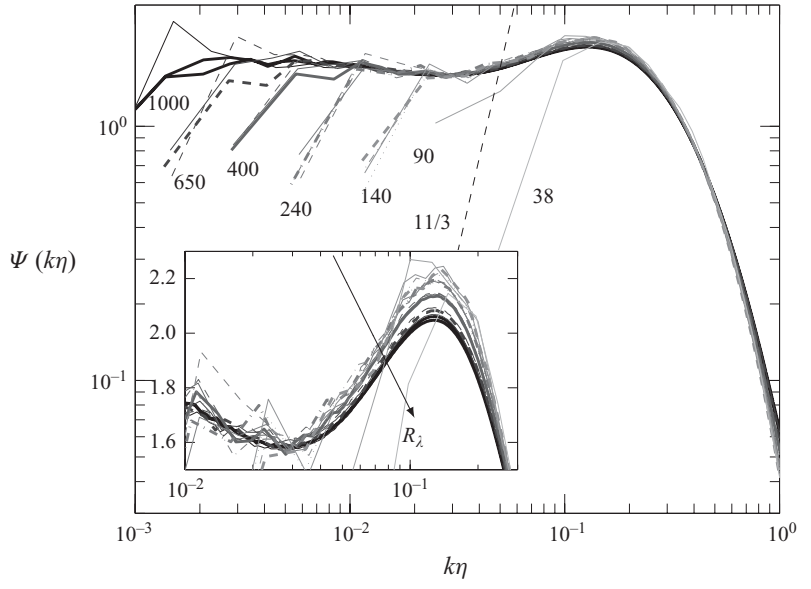

FIGURE 1. Compensated spectra for $R_\lambda \approx 38$, 90, 140, 240, 400, 650 and 1000 in different tones (as indicated in the figure) with resolutions $k_{max}\eta \approx 1.5$ (solid lines), 3 (dashed lines), 6 (dashed–dotted lines) and 12 (dotted lines). Thin and thick lines correspond to EP and FEK forcing schemes, respectively (see text). Inset: the compensated spectra in log-linear scales. The dashed line with slope 11/3 represents complete 'thermalization' (see § 2).

Substantial efforts have been devoted to determining C_K in experiments (e.g. Sreenivasan 1995) and simulations (e.g. Yeung & Zhou 1997). A typical procedure for estimating C_K is to plot the 'compensated' spectrum

$$\Psi(k\eta) \equiv \frac{E(k)}{\langle\epsilon\rangle^{2/3}k^{-5/3}}, \tag{1.3}$$

for $kL \ll 1$ and seek a plateau, whose height is taken as C_K. However, it is hard to obtain accurate values of C_K in experiments and simulations. We discuss two operational sources of uncertainty by referring to figure 1 (and relegating a discussion of its other details to the following sections).

First, at any finite Reynolds number, a perfectly horizontal region does not exist in any significant part of the compensated spectrum, so the determination of C_K is ambiguous to some extent. This difficulty, especially evident in the compensated spectrum plotted on the linear scale (see inset), may well be due to inertial range intermittency, whose effects are noticeable even in second-order statistics (Kaneda *et al.* 2003). Due to the intermittent character of the energy dissipation rate, corrections to the inertial range slope in (1.2) of the form $k^{-5/3-\beta}$ ($\beta > 0$) have been proposed. However, assessing the appropriateness of this formulation, using either experimental or numerical data, requires a simultaneous determination of two parameters C_K and β. Furthermore, β is expected to be of the order of 1.5 % of the slope in (1.2) (see Sreenivasan & Kailasnath 1993) and may escape definitive detection in experimental (e.g. Praskovsky & Oncley 1997) or numerical simulations (see below), often leading to inconsistent results. Perhaps for reasons suggested in Bailey *et al.* (2009), the high-wavenumber end of the $k^{-5/3}$ scaling occurs for $k\eta$ between 10^{-2} and 10^{-1}. The second difficulty is the behaviour of the spectrum around $k\eta = O(1)$ (the 'near-dissipation'

range) where viscous effects are important: the function $f(k\eta)$ does not decrease monotonically with increasing wavenumbers but shows a spectral 'bump', known as the bottleneck. At low enough Reynolds numbers (say $R_\lambda \approx 40$, which is typical of the early measurements in grid turbulence), the temptation has been to read the value C_K from the peak in the bottleneck region, with the expectation that it is the harbinger of the high-Reynolds-number plateau in (1.3). Figure 1 shows that the peak has nothing to do with the inertial range.

At least in the traditional picture, the inertial range and the near-dissipation ranges separate from each other at very high Reynolds numbers, though it is conceivable that this separation of scales might not be a precise description at any Reynolds number. If, however, the traditional picture is correct, the two difficulties just mentioned are distinct and it is to be expected that the Kolmogorov constant (if it exists) can be determined without the influence of the bottleneck. At moderate Reynolds numbers, however, a proper determination of C_K is tied to the understanding of the bottleneck effect, which is the subject of this study. The bottleneck, which was captured in an analytical derivation in Qian (1984), has been interpreted by Falkovich (1994) as a consequence of viscous suppression of high-wavenumber modes, diminishing energy transfer and piling up energy at the boundary between inertial and dissipative regions, and leading to the spectral form $(k\eta)^{4/3}\ln^{-1}(k\eta)$ (see also e.g. Lohse & Müller-Groeling 1995; Martinez *et al.* 1997). Yakhot & Zakharov (1993), on the other hand, used Clebsch variables to derive a k^{-1} continuation at high wavenumbers of the $k^{-5/3}$ region. The physical mechanism suggested in Yakhot & Zakharov (1993) is based on 'waves' emitted at the smallest scales due to viscous effects generating an inverse cascade. Kurien, Taylor & Matsumoto (2004) proposed a $k^{-4/3}$ scaling in the bottleneck region associated with the dynamics of helicity. A different approach was used in Verma & Donzis (2007) where the bump was attributed to an insufficiently wide range of scales. Bershadskii (2008) related a k^{-1} scaling to non-local interactions with large scales and, based on a perturbation approach, suggested an exponential roll-off of the spectral density at higher wavenumbers. Frisch *et al.* (2008) used hyperviscous equations and closures to argue that the case of ordinary dissipation (i.e. the Laplacian of velocity components) leads to 'incomplete thermalization', whose asymptotic scaling, given by k^2, for the three-dimensional spectrum shows the bottleneck. Other *ad hoc* functional forms have also been proposed in the literature (e.g. Cerutti & Meneveau 2000; Kang, Chester & Meneveau 2003; Meyers & Meneveau 2008).

As already mentioned, the difficulties cited earlier in estimating C_K may be thought to vanish at very high Reynolds numbers. Indeed, geophysical flows which reach very high Reynolds numbers (e.g. Kaimal *et al.* 1972; Dhruva, Tsuji & Sreenivasan 1997; Praskovsky & Oncley 1997; Sreenivasan & Dhruva 1998; Tsuji 2004) seem to support this view, but they are often subject to effects of non-stationarity of the large scales. Controlled laboratory flows are limited to moderate Reynolds numbers, and usually subject to the use of Taylor's frozen-flow hypothesis, surrogates for quantities that are difficult to measure (e.g. full energy dissipation) as well as limited spatial resolution. Most of these problems can be obviated in direct numerical simulations (DNS). Though the DNS has been historically limited to low Reynolds numbers with narrow inertial range, the relentless growth in computational power over the last 50 years makes it possible to attain Reynolds numbers high enough to observe a clean inertial scaling and, at the same time, resolve small scales with sufficient accuracy for statistics of moderate order (Watanabe & Gotoh 2007; Donzis, Yeung & Sreenivasan 2008*b*). It has been argued recently (e.g. Yakhot & Sreenivasan 2005; Donzis *et al.*

2008*b*) that the resolution commonly employed in the DNS is inadequate, but this can be checked by repeating the calculations with improved resolution.

The aim of this paper is to use the DNS data to address the scaling of the bottleneck effect and determine the Kolmogorov constant as accurately as possible. Our focus will be the three-dimensional spectrum, obtained with the energy dissipation and related quantities calculated properly, because it presents a stronger bottleneck than the one-dimensional spectrum (Dobler *et al.* 2003). Furthermore, our large DNS database (summarized in Donzis, Yeung & Pekurovsky 2008*a*; Donzis & Yeung 2009), comprising a wide range of Reynolds numbers, different resolutions and forcing schemes, allows us to address the sensitivity of the results to varied conditions.

The DNS data are obtained using a massively parallel pseudo-spectral code which achieves excellent performance on $O(10^4)$ processors up to 4096^3 grid points with the Taylor–Reynolds number up to $R_\lambda \approx 1000$. Here, we show results using the stochastic forcing of Eswaran & Pope (1988) – denoted below as EP – as well as a deterministic scheme described in Donzis & Yeung (2009) – denoted below as FEK – which, in essence, keeps the energy in the lowest wavenumbers fixed. For these two forcing schemes, the wavenumbers affected by forcing are confined to within a sphere $k < k_F$, where k_F is of order 2 or 3. To address the effect of small-scale resolution, we will present results at $k_{max}\eta \approx 1.5$, 3, 6 and 11, where $k_{max} = \sqrt{2}/3N$ is the highest resolvable wavenumber in a domain of size $(2\pi)^3$ with N^3 grid points.

2. The bottleneck effect

The three-dimensional spectra in figure 1 were computed for different Reynolds numbers, resolutions and forcing schemes. Due to the variabilities within the forcing schemes (especially EP), the data have been time averaged over several eddy-turnover times. Except at small wavenumbers, the spectra collapse well. The spectral bump for all Reynolds numbers is centred around $k\eta \approx 0.13$, consistent with previous findings (e.g. She & Jackson 1993). The higher the Reynolds number, the more extensive is the nearly flat region (the 'inertial range') in the compensated spectrum; the inertial scaling is essentially absent for $R_\lambda < 140$. The effect of the forcing and resolution appears to be negligible in both the inertial and dissipative ranges; most of the differences at small wavenumbers occur around the forcing wavenumbers where statistical convergence is problematic. However, since the focus of this paper is on small scales, we will not analyse the large scales in any detail here.

To quantify the properties of the bottleneck, we compute the location, k_p, and the height, Ψ_p, of the bump for each curve in figure 1: $\Psi(k_p\eta) \equiv \Psi_p$. Except for the lowest Reynolds numbers, the location of the bump in Kolmogorov variables, i.e. $k_p\eta$, appears to be independent of R_λ, the forcing scheme and the resolution in the simulations (figure 2). For $R_\lambda \approx 38$ and 90, a prominent bottleneck appears without any sign of an inertial range, which suggests that the bottleneck is not simply a consequence of the inertial range dynamics. We shall return to this consideration in § 6.

Although the location of the bump is independent of R_λ, its height decreases systematically with R_λ, as shown in the inset of figures 1 and 3, following a power law of the form $\Psi_p \sim R_\lambda^{-\gamma}$ with $\gamma = 0.04$; the data are, however, not inconsistent with a logarithmic dependence (Verma & Donzis 2007). Since the spectral bump occurs before the inertial range emerges, non-local effects may play a significant role in bottleneck effects.

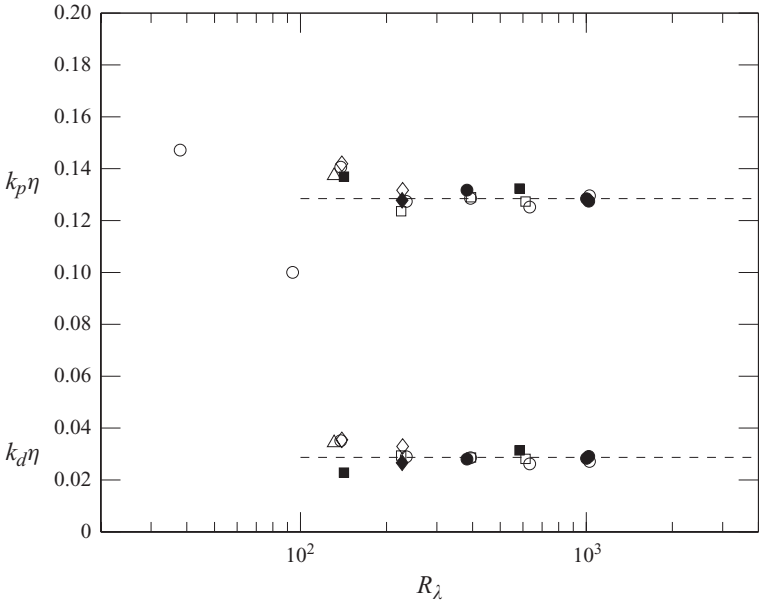

FIGURE 2. Wavenumbers k_p and k_d where Ψ attains its local maximum and minimum, respectively, towards the end of the inertial range. Circles, squares, diamonds and triangles are for $k_{max}\eta \approx 1.5$, 3, 6 and 11, respectively. Open and filled symbols correspond to EP and FEK forcing schemes, respectively. Dashed lines at $k_p\eta = 0.13$ and $k_d\eta = 0.029$ are average values for $R_\lambda \geqslant 240$.

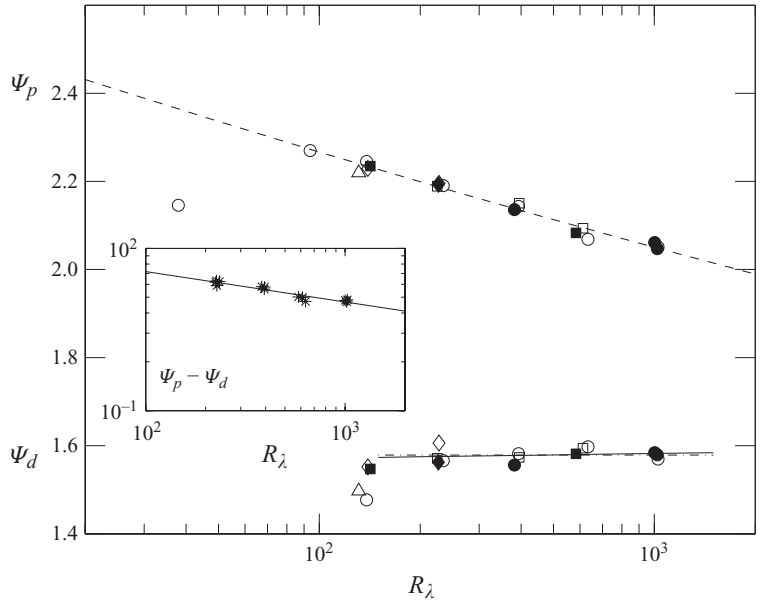

FIGURE 3. The height of the spectral bump Ψ_p (upper plot) and the Kolmogorov constant computed as the local minimum prevailing before the bump, Ψ_d (lower plot). Circles, squares, diamonds and triangles are for $k_{max}\eta \approx 1.5$, 3, 6 and 11, respectively. Open and filled symbols correspond to EP and FEK forcing schemes, respectively. Dashed and solid lines are best fits for data at $R_\lambda \geqslant 140$ and $R_\lambda \geqslant 240$, respectively. The dashed–dotted line at $\Psi_d = 1.58$ is the average for $R_\lambda \geqslant 240$. The inset shows that, for $R_\lambda > 240$, $\Psi_p - \Psi_d$ can be approximated by $R_\lambda^{-0.2}$.

We have also examined one-dimensional spectra (not shown) and found that the (smaller) bottleneck effect also decreases roughly as $R_\lambda^{-0.04}$ for both longitudinal and transverse spectra.

The most important point of the discussion so far is that the fundamental assumption embodied in (1.1) (or (1.2)) should be modified to

$$\frac{E(k)}{u_\eta^2 \eta} = F(k\eta, R_\lambda), \quad k \gg 1/L. \tag{2.1}$$

It is clear that the form of (1.1) or (1.2) (e.g. Qian 1984; Yakhot & Zakharov 1993; Falkovich 1994; Bershadskii 2008) cannot fully explain the observed behaviour, at least for finite R_λ, unless the 'constants' in the different models are allowed to depend on R_λ (Barenblatt & Goldenfeld 1995).

An alternative form of (2.1) would be $E(k)/(u_\eta^2\eta) = F(k\eta, L/\eta)$, which has been used to account for intermittency corrections in the inertial range where, as mentioned in § 1, a scaling of the form $(k\eta)^{-5/3}(kL)^{-\mu/9}$ is thought to exist with a Reynolds-number-independent intermittency exponent μ (see e.g. Monin & Yaglom 1975). The classical estimate $L/\eta \approx (A/15)R_\lambda^{3/2}$ ($A \equiv \langle\epsilon\rangle L/u'^3$ being a constant for $R_\lambda \gtrsim O(100)$; see e.g. Donzis, Sreenivasan & Yeung 2005) allows us to write $E(k)/(u_\eta^2\eta) \propto (k\eta)^{-(5/3+\mu/9)} R_\lambda^{-\mu/6}$. Using the generally accepted value of $\mu \approx 0.25$ (Sreenivasan & Kailasnath 1993), the Reynolds number dependence turns out to be $\mu/6 \approx 0.042$, which is close to the value of γ for Ψ_p, as observed in Meyers & Meneveau (2008). However, this intermittency correction is valid in the inertial range and extending its applicability to dissipative scales is not strictly justified. Furthermore, such a correction would complicate the interpretation of the Kolmogorov constant, as we will discuss in the next section.

A recent explanation for the bottleneck, due to Frisch *et al.* (2008), is that the spectral bump is related to the thermalization process that occurs in truncated hyperviscous Navier–Stokes equations. Their results, based specifically on the EDQNM, the standard notation for eddy damped quasi-normal Markovian, assumptions, show a spectral bump in the neighbourhood of the truncation wavenumber and a spectral 'dip' preceding the bump. Both the bump and dip were shown to increase with increasing power of the Laplacian in the viscous term. (The dip was present only when the power of the Laplacian was greater than unity.) We have computed the local minimum of $\Psi(k\eta)$ at wavenumbers preceding the bump location; this dip, evident in experiments (e.g. Tsuji 2004) and simulations (e.g. figure 5 of Kaneda *et al.* 2003) alike, will be denoted here by Ψ_d and its location by k_d. Details of the region around the local minimum ($k\eta \approx 3 \times 10^{-2}$) can be seen in figure 4(a) for spectra at different Reynolds numbers. The values of Ψ_d obtained from our simulations are collected in figure 2 only for $R_\lambda \geqslant 140$ since no minimum is evident for lower Reynolds numbers; Ψ_d remains approximately constant. If we use only the data at $R_\lambda \geqslant 240$ for the fit, the slope turns out to be practically zero (solid line), in agreement with the classical K41 inertial range phenomenology. For reference, figure 1 includes a dashed line with slope 11/3, corresponding to complete thermalization. The data do not support this trend. It is clear from figure 2 that the location of the dip, $k_d\eta$, is independent of the Reynolds numbers and that Ψ_p decreases with R_λ.

3. The Kolmogorov constant

The numerical value of C_K and its Reynolds number trends are unclear in past data. Some studies (Praskovsky & Oncley 1994; Mydlarski & Warhaft 1998; Mininni,

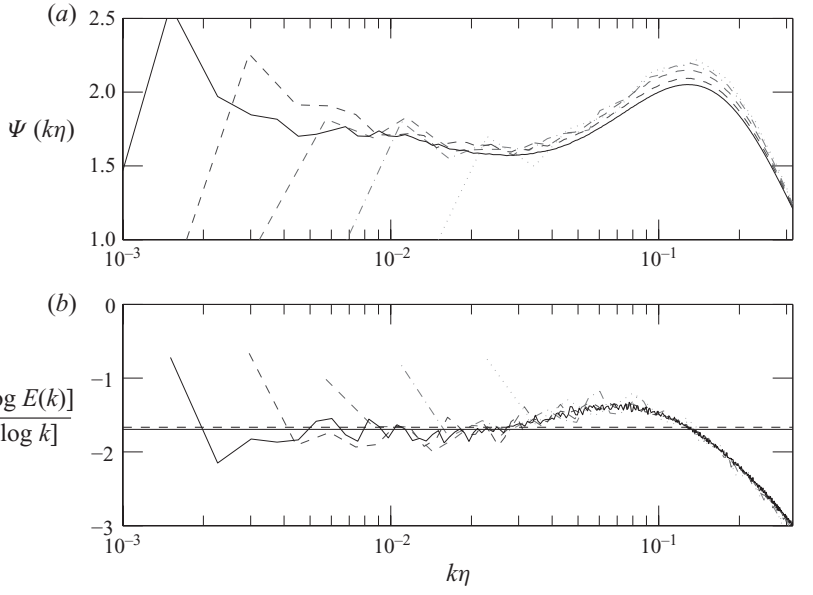

FIGURE 4. (*a*) Compensated spectrum at $R_\lambda \approx 140$, 240, 400, 650 and 1000 at the highest resolutions available for each Reynolds number. (*b*) The logarithmic derivative $\mathrm{d}[\log E(k)]/\mathrm{d}[\log k]$ for these same cases. Dashed and solid horizontal lines at $-5/3$ and $-(5/3+\mu/9)$ with $\mu = 0.25$ are for reference. The notations for spectra correspond to those in figure 1.

Alexakis & Pouquet 2008) and theories (Barenblatt & Goldenfeld 1995) suggest that C_K decreases with R_λ. The data from Tsuji (2004), at very high $R_\lambda \approx 17\,000$, yield a three-dimensional Kolmogorov constant of $C_K \approx 1.9$, which is higher than those at lower R_λ (e.g. Praskovsky & Oncley 1994; Mydlarski & Warhaft 1998). The data collected in Sreenivasan (1995), on the other hand, suggest an essentially constant value of C_K beyond R_λ of about 100, as can also be inferred from simulations in Kaneda *et al.* (2003) and Gotoh, Fukayama & Nakano (2002) and from recent experiments of Welter *et al.* (2009).

It is most likely the case that these conflicting conclusions are the result of inconsistent procedures followed in the determination of C_K. At low Reynolds numbers, the Kolmogorov constant is estimated by the peak in the compensated spectrum with the anticipation that it is the incipience of the expected flat region. The practice is akin to drawing on the spectrum a tangent with the slope of $-5/3$, again with the expectation that, as the Reynolds number increases, the spectrum will expand along the tangent. The purported magnitudes of C_K thus determined are unreliable and the claims of Reynolds number dependence based on this and comparable practices lack conviction, especially when data from different sources are considered.

One may now incorporate intermittency corrections and write (1.2) as $E(k)/(u_\eta^2\eta) = C'_K(k\eta)^{-5/3}(kL)^{-\beta} = C'_K R_\lambda^{-3\beta/2}(k\eta)^{-5/3-\beta}(A/15)^{-\beta}$, where C'_K may be different from C_K in (1.2) (see e.g. Monin & Yaglom 1975). If the 'Kolmogorov constant' is computed as the prefactor to the term containing $k\eta$ to some power, say $C''_K = C'_K R_\lambda^{-3\beta/2}(A/15)^{-\beta}$, a decrease in C''_K with R_λ does not imply that trend for C'_K (or C_K). The determination of C_K is thus linked to the determination of the intermittency exponent in the inertial range. This problem survives even when

one uses 'logarithmic derivatives' (i.e. $\mathrm{d}[\log E(k)]/\mathrm{d}[\log k]$) and the independent term of $\log E(k) = \log(C'_K \langle\epsilon\rangle^{2/3} L^{-\beta}) - (5/3 + \beta)\log k$. The difficulties are clearly seen in figure 4 where we show $\Psi(k\eta)$ and $\mathrm{d}[\log E(k)]/\mathrm{d}[\log k]$ for different Reynolds numbers at the highest resolution available. Determining departures from 5/3 (the dashed line in part *b* of the figure) will be clearly biased by the choice of the fitting range at both ends of the nominal inertial range. As already remarked, this has caused the overestimation of C_K at lower Reynolds numbers (Yeung & Zhou 1997). To highlight the difficulties in trying to compute departures accurately, we also include $-(5/3+\mu/9)$ in figure 4(*b*), which is nearly indistinguishable from $-5/3$. Thus, taking account of classical intermittency corrections in the inertial range does not alter the picture too much for the present data.

A possible interpretation of the results follows. Ignoring intermittency, the Kolmogorov spectrum is written as $E(k)/(u_\eta^2\eta) = C_K(k\eta)^{-5/3}$. Thus, the Kolmogorov constant can be interpreted as the spectral level at $k\eta = 1$, which, within the theory, marks the viscous end of the inertial range. This procedure of computing quantities in the dissipative range by allowing inertial range scaling down to Kolmogorov scale, though not completely justified for all quantities of interest, is not new and has been used extensively in the literature (see e.g. Nelkin 1990; Yakhot & Sreenivasan 2005, among others). However, the bottleneck effect, which is not within the purview of K41, spoils this simplicity. Therefore, it is reasonable to look for the spectral level 'just before' the bump begins to rise (this being the largest wavenumber which may be expected to be unaffected by the bottleneck). This is, in fact, how Ψ_d was computed above. It provides an unambiguous – and, presumably, the correct – way of determining the Kolmogorov constant without arbitrary specifications of scaling ranges or particular choices of intermittency corrections. As seen in figure 3, the determination of Ψ_d proposed here leads to a constant independent of the Reynolds number. The average in the range $R_\lambda \geqslant 240$ is $C_K = 1.58$. This is also consistent with a reading of the figures in Aoyama *et al.* (2005) (for example).

We further note that if intermittency corrections were used to compensate the spectra in such a way that the R_λ-dependency of the bottleneck vanishes, then the Reynolds number dependency would reappear in inertial range quantities. This is clear from the different scaling seen for Ψ_d and Ψ_p in figure 2. If no departures from $k^{-5/3}$ existed, our proposal will also yield the same C_K as determined using traditional methods.

4. Bottleneck in physical space: structure functions

In isotropic turbulence, the three-dimensional energy spectrum is related uniquely to second-order structure functions (see e.g. Monin & Yaglom 1975). At very small separations, the viscous (analytical) scaling is given by $D_L(r)/u_\eta^2 = (1/15)(r/\eta)^2$ and $D_T(r)/u_\eta^2 = (2/15)(r/\eta)^2$, where well-known isotropic relations have been used. Here, D_L and D_T are the longitudinal and transverse structure functions, respectively. In the inertial (singular) range, a scaling of the form $D_L \sim r^{\zeta_2}$ is usually sought. One may expect that the bottleneck effect in spectral space will have a corresponding manifestation in physical space near the transition between viscous and inertial regions for $D_L(r)$ and $D_T(r)$, but there is little discussion of this aspect in the literature. In fact, Dobler *et al.* (2003) argued that localized features such as the bottleneck in wavenumber space will make it sufficiently non-local, and hence, unnoticeable, in physical space.

The classical study of the transition region by Batchelor (1951) applies well to both longitudinal and transverse structure functions (see e.g. Benzi *et al.* 1993). The relevant expression is

$$\frac{D_B(r)}{u_\eta^2} = K \frac{(r/\eta)^2}{[1 + (c_B\ r/\eta)^q]^{(2-\zeta_2)/q}}, \tag{4.1}$$

with $K = 1/15$ for the longitudinal and $2/15$ for the transverse structure functions, and $q = 2$. The parameter c_B is determined empirically (see Stolovitzky, Sreenivasan & Juneja 1993). The spectrum obtained by transforming $D_B(r)$ to Fourier space does show a spectral bump (Sirovich, Smith & Yakhot 1994). On the other hand, a model spectrum without a bump can be transformed to physical space, leading to a more gradual transition between analytical and singular regions, as was shown by Lohse & Müller-Groeling (1995), who also concluded that the rapidity of transition between these ranges is the manifestation of the spectral bump. But Batchelor's expression does not depend on the Reynolds number when expressed in terms of Kolmogorov variables and is thus at variance with the findings in the previous section.

It is therefore useful to investigate how the spectral bump transforms itself in physical space. In figure 5 we show $D_L(r)$ and $D_T(r)$ normalized according to K41 (i.e. with $\zeta_2 = 2/3$) using DNS data at three Reynolds numbers. An inspection of the insets (which show a detailed view of this transition between the asymptotes $r^{4/3}$ and r^0) shows a systematic though weak Reynolds number dependence – this being stronger for transverse structure functions. We thus indeed have

$$\frac{D_{L/T}(r)}{u_\eta^2} = G(r/\eta, R_\lambda), \tag{4.2}$$

instead of a Reynolds-number-independent universal function. In the singular range, we see a weak departure from the plateau shown by the dashed line of figure 5, indicating anomalous scaling with $\zeta_2 > 2/3$ (see e.g. Chen *et al.* 2005, and more below). The data at $R_\lambda \approx 400$ for two different forcing schemes show that details of large-scale forcing do not produce observable changes in the transition region.

To assess more directly the Reynolds number effects on the transition, we show in figure 6 the transverse structure functions at different Reynolds numbers normalized by $D_T(r/\eta, 1000)$ as reference. For small and large r, we expect structure functions to approach analytical and singular scaling, respectively. The figure shows that at intermediate scales, the ratio is largest at low R_λ with a maximum around $r/\eta \approx 20$. Longitudinal structure functions (not shown here) exhibit the same but weaker trend. The numerical value of the structure functions so normalized at the scale of largest difference is shown in figure 7 as a function of R_λ. The results in figures 5–7 show that the transition is more rapid at low Reynolds numbers. The smoother transition in physical space and a reduction of the bottleneck in spectral space at high Reynolds numbers are complementary and consistent with Lohse & Müller-Groeling (1995).

We have also computed the three-dimensional structure function $D(r)$ which, in an isotropic situation, like the present, can be written as $D(r) = 3D_L(r) + r\ \mathrm{d}D_L(r)/\mathrm{d}r$. Since the computation of $D(r)$ requires differentiation with respect to the separation r and only discrete values are available from simulations, we have interpolated our results to a finer grid using splines and applied a high-order finite difference operator. We have confirmed that a smoother transition occurs at high R_λ similar to those seen in previous figures for longitudinal and transverse structure functions. The Reynolds

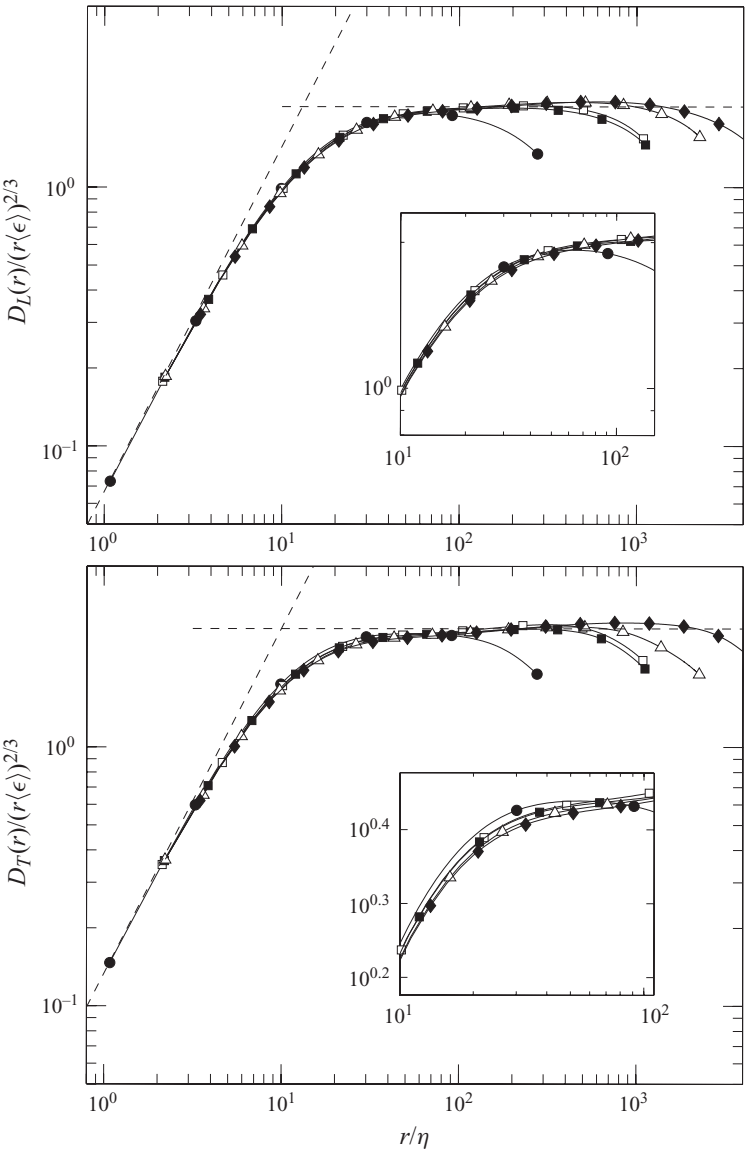

FIGURE 5. Second-order structure functions $D_L(r)$ and $D_T(r)$ at $R_\lambda \approx 140$ (circles), 400 (squares), 650 (triangles) and 1000 (diamonds). Open and filled symbols are for EP and FEK forcing schemes, respectively. Dashed lines: asymptotes $r^{4/3}$ and r^0 for analytical and singular range, respectively. Inset: detail of the transition region.

number dependence of $D(r)$ evaluated at $r/\eta \approx 20$ is $R_\lambda^{-0.024}$, which lies between the values for $D_L(r)$ and $D_T(r)$ (see figure 7).

Equation (4.1) has been used widely in the literature (e.g. Stolovitzky *et al.* 1993; Lohse 1994; Sirovich *et al.* 1994; Meneveau 1996; Chevillard *et al.* 2006). However, it is necessary to incorporate the Reynolds number dependence for it to conform to (4.2). If the analytical and singular ranges are assumed to be universal and the functional form (4.1) is to be retained, the rapidity of the transition is controlled only by the parameter q. We have used (4.1) to fit the structure functions in figure 5, and summarize the results in figure 8 with $\zeta_2 = 0.67$. To avoid the contamination by large scales, the fitting

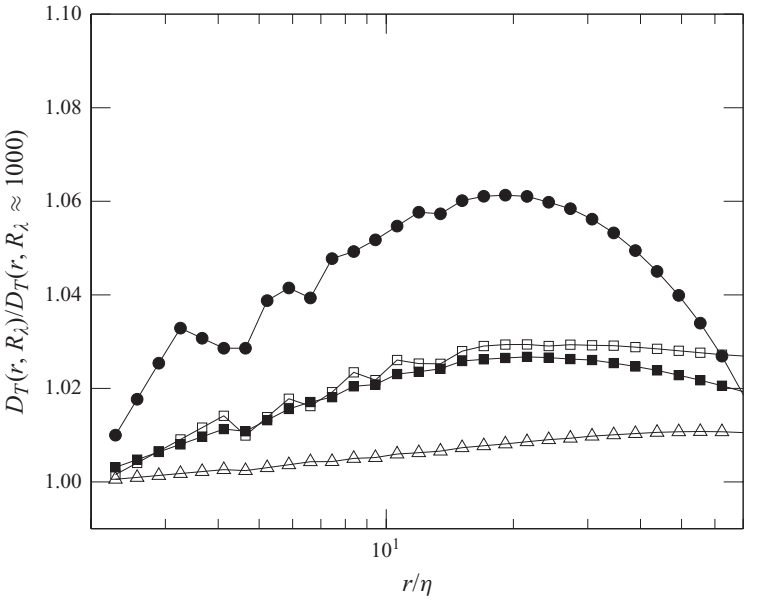

FIGURE 6. The ratio between structure functions $D_T(r/\eta, R_\lambda)$ and $D_T(r/\eta, 1000)$ with $R_\lambda \approx 140$ (circles), 400 (squares) and 650 (triangles). Open and filled symbols are for EP and FEK forcing, respectively.

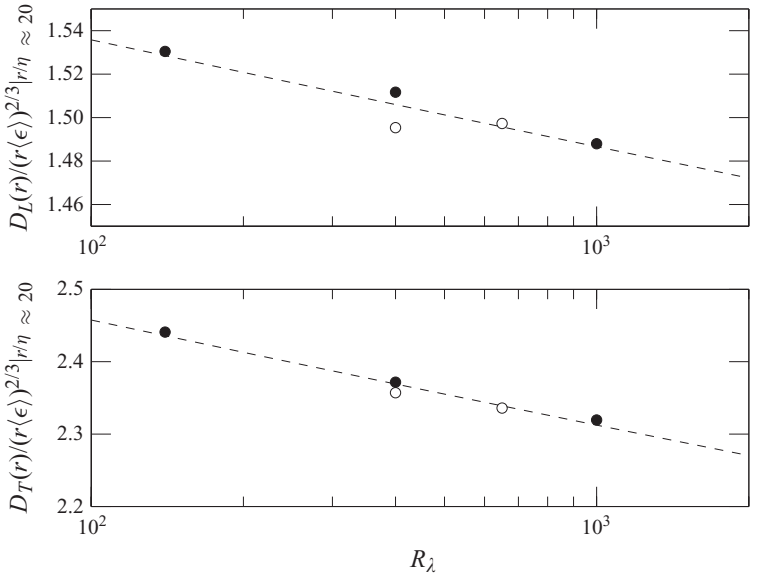

FIGURE 7. Normalized second-order structure functions at the scale of maximum departure. Open and filled symbols are for EP and FEK forcing, respectively. Dashed lines correspond to best fits of the form $R_\lambda^{-0.014}$ and $R_\lambda^{-0.026}$.

range was limited to $r/\eta \leqslant 70$. (The best-fit coefficients are robust against reasonable variations in this limit. For example, increasing the range to $r/\eta < 100$ changes the value of c_B by less than 1 %.) Figure 8(a) shows that c_B is independent of R_λ with average values of 0.076 and 0.102 for longitudinal and transverse structure functions, respectively. By means of isotropic relations (Monin & Yaglom 1975), one can use

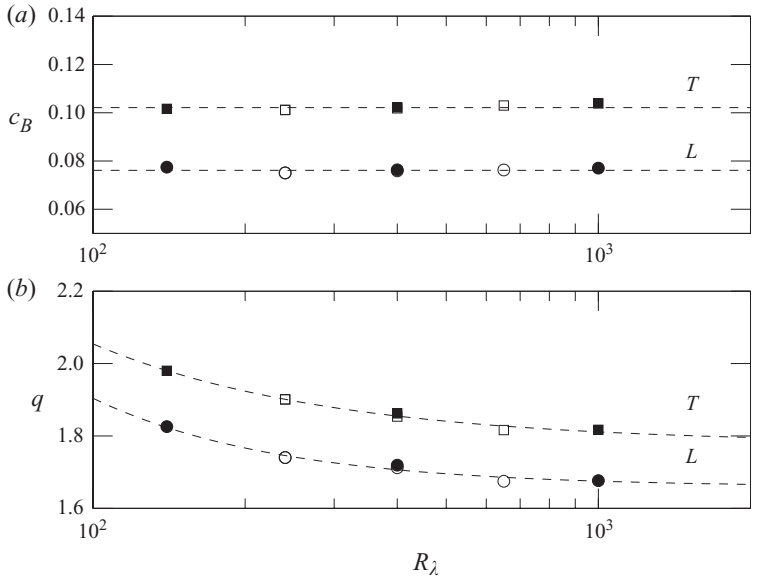

FIGURE 8. Constants c_B and q as functions of R_λ for longitudinal (circles) and transverse (squares) structure functions. Open and filled symbols are for EP and FEK forcing schemes, respectively. Dashed lines: (a) mean value of c_B at 0.076 and 0.102; (b) best fits of the form $q_L = \alpha_L R_\lambda^{-\beta_L} + \gamma_L$ and $q_T = \alpha_T R_\lambda^{-\beta_T} + \gamma_T$ with $(\alpha_L, \beta_L, \gamma_L) = (32.6, 1.06, 1.65)$ and $(\alpha_T, \beta_T, \gamma_T) = (19.4, 0.92, 1.78)$.

c_B for the longitudinal case to obtain $C_K = (1/4.02)(55/18)(1/15)c_B^{\zeta_2 - 2} = 1.56$ which is, therefore, independent of R_λ as well. This value is also in agreement with that obtained from the spectrum (see figure 3), but the procedure itself depends on the value of the scaling exponent ζ_2, whose determination is ambiguous when a clear scaling range is not present.

In figure 8(b) we show q as a function or R_λ. Its unambiguous decrease with the Reynolds number, at least for low and moderate values, confirms the conclusion that the transition at high Reynolds numbers is smoother, which is the manifestation of a milder spectral bump. The data can be fitted by an expression of the form $q_L = \alpha_L R_\lambda^{-\beta_L} + \gamma_L$, with the suffix L indicating the longitudinal case. A similar fit exists for transverse structure functions. The high-Reynolds-number asymptotes are given by $\gamma_L = 1.65$ and $\gamma_T = 1.78$. It is interesting that while the shape of $D_{L/T}(r)$ at the transition changes with R_λ, c_B and, therefore, C_K, remain constant, resembling the behaviour of Ψ_p and Ψ_d.

Since the conclusions drawn for longitudinal and transverse structure functions also apply to the three-dimensional $D(r)$, the corresponding figures are not shown here. Equation (4.1) can represent the data quite well with q varying with the same functional form as that for the longitudinal and transverse structure functions but with different numerical coefficients. In this case, we find $q = 241 R_\lambda^{-1.39} + 1.74$.

5. Correspondence between wavenumber space and physical space

We have shown in figure 1 that the spectral bump is centred around $k\eta \approx 0.13$. From the qualitative correspondence $k \sim 1/r$, we might expect the transition region from analytical to singular parts of the structure functions to lie roughly around $r/\eta \sim O(10)$. Indeed, the intersection of the asymptotes from the two regions, shown

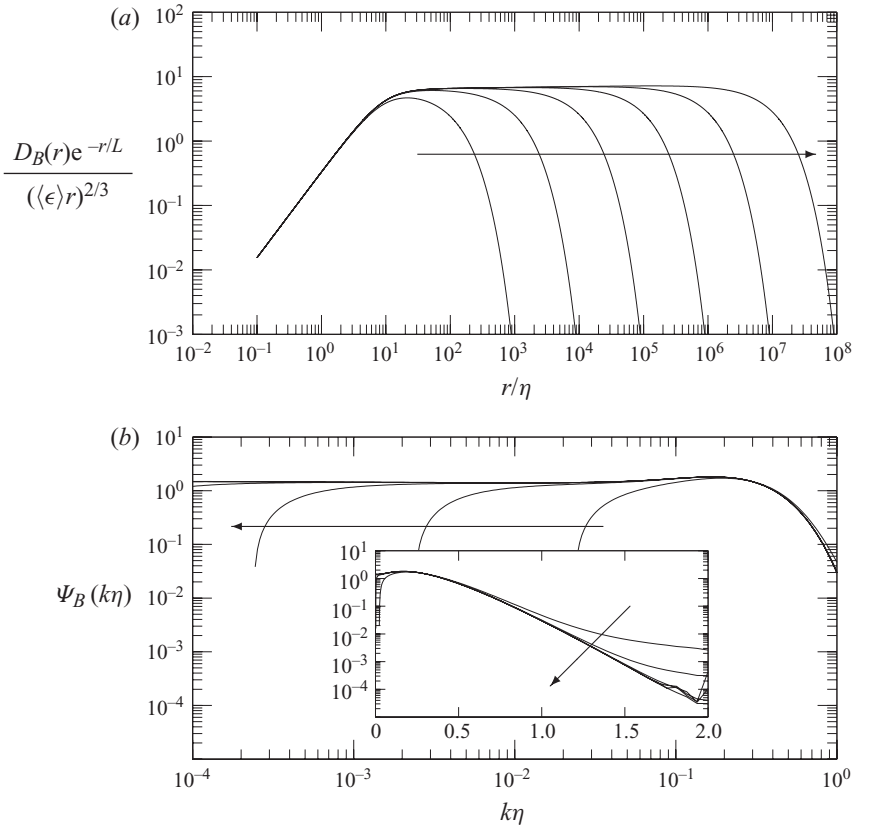

FIGURE 9. (*a*) The structure function model given by $D_B(r)\exp(-r/L)$ with $\zeta_2 = 0.68$ and $q = 2$. (*b*) Compensated energy spectrum corresponding to structure functions in (*a*). Different lines correspond to $L/\eta = 10^2, 10^3, \ldots, 10^7$, increasing values of L/η (or R_λ) indicated by the direction of the arrow. The inset plots the spectra in log-linear coordinates.

in figure 5, roughly bear out this expectation. However, as mentioned in Dobler *et al.* (2003), local features in one space are non-local in the other. This is easily seen from the integral relations between $D(r)$ and $E(k)$ which, for isotropic turbulence, are given by $E(k) \propto \int_0^\infty kr \sin(kr) D(r)\,\mathrm{d}r$ and $D(r) \propto \int_0^\infty (1 - \sin(kr)/kr) E(k)\,\mathrm{d}k$ (see e.g. Monin & Yaglom 1975). The lack of knowledge on the shape of $E(k)$ and $D(r)$ and the oscillatory nature of the integrands make it difficult to be precise about the correspondence between the bottleneck effects in k and r spaces.

Nevertheless, we can use (4.1) to obtain analytical expressions to assess this correspondence. Since (4.1) grows without bound as $r \to \infty$, one has to make some assumption on this asymptotic behaviour. Different such assumptions have been made in the literature (Sirovich *et al.* 1994; Lohse & Müller-Groeling 1996; Aivalis *et al.* 2002), but we assume a simple form that lends itself to analytical treatment. In particular, the downturn for large values of r observed in figure 5 is modelled by multiplying (4.1) by $\exp(-r/L)$. Figure 9(*a*) shows the incorporation of this functional form for various L/η (or R_λ). Although this form is not strictly correct since $D_{L/T}(r)$ should approach a constant for large r, it will serve to draw some useful conclusions. The corresponding normalized energy spectrum, $\Psi_B(k)$, obtained by solving the integral relation between $D(r)$ and $E(k)$, is quite intricate and involves

hypergeometric and Bessel functions. In figure 9(*b*) we show the result for the cases considered in figure 9(*a*).

By construction, the widening of the inertial range is the only real-space change occurring as L/η increases. In spectral space, one observes not only a corresponding widening of the inertial range but also, and more interestingly, a strong dependence of the far dissipation range on L/η. Even though this effect weakens when the separation of scales is large enough – as is clear from the inset of figure 9(*b*) where we plot the spectra in log-linear scales – it is apparent that changes in the form of structure functions at large separations influence the spectrum at dissipative scales, making it difficult to identify the bottleneck effects localized around a wavenumber k with similar effects around $1/k$ in real space. Though this result was obtained from a model structure function, similar considerations could be applied to experimental and numerical data.

As a final point, we note that the behaviour present in the inset of figure 9(*b*) appears to show an opposite trend to that from DNS data as R_λ increases (see e.g. figure 1). Although genuine concerns can be raised about the accuracy of the data at very high wavenumbers (close to $k_{max}\eta$), the present results suggest that the large scales in physical space can show a 'qualitative' change of behaviour at high wavenumbers. We stress, nevertheless, that highly resolved simulations over a wider range of Reynolds numbers will be needed to make more definite statements.

In summary, any assessment of the features in one space cannot be translated to the other in a straightforward manner; both representations have to be examined. In particular, the definitions of large and small scales in one space do not correspond to the same definition in the other space simply through the use of $k \sim 1/r$. Although this result does not immediately imply that large scales in real space influence the spectral bump, we explore this possibility in the next section.

6. Discussion

Extrapolation of the best fits in figure 3 for Ψ_p and Ψ_d suggests that the bottleneck would essentially disappear at $R_\lambda \sim O(2 \times 10^5)$. Alternatively, the inset of figure 3 shows the difference $\Psi_p - \Psi_d$ as a function of R_λ. A power law with the exponent of -0.2 (solid line) is also consistent with the data, showing that the bottleneck disappears gradually and would be negligible at $R_\lambda \sim 2 \times 10^5$. This Reynolds number is beyond today's computational capabilities. Atmospheric flows do achieve such Reynolds numbers, though results from these flows are limited to one-dimensional spectra (which are known to possess smaller spectral bumps). If the bottleneck disappears only at very large Reynolds numbers, all finite-Reynolds-number theories must necessarily incorporate it. We have already suggested above that non-local transfer may play a role in such a theory. We now make this statement more quantitative.

The local energy transfer from a wavenumber k in the inertial range to higher wavenumbers can be estimated by the energy $E(k)k$ divided by the cascade time scale $\langle\epsilon\rangle^{-1/3}k^{-2/3}$. The diffusive loss of energy is of the order $E(k)k/(k^{-2}\nu^{-1})$, where we have used $k^{-2}\nu^{-1}$ for the diffusive time scale. On dimensional grounds, the effect of non-local transfer from large scales, say L with characteristic velocity u' (e.g. the r.m.s. velocity), to wavenumber k can be estimated as $u'[E(k)k]/L$. It is relevant to note that simulations of Mininni *et al.* (2008) suggest that the energy transfer from large scales does not vanish at high wavenumbers for fixed R_λ, but approaches a constant. This asymptote, however, does decrease with R_λ. We can now combine the

three contributions weighted by constants c_1, c_2 and c_3, all of the order unity, and equate the sum to $\langle\epsilon\rangle$, which is the transfer of energy directed by the large scales. The result can be put in non-dimensional form as

$$\Psi(k\eta) = [1/c_1 + (k\eta)^{4/3}/c_2 - c_3(k\eta)^{-2/3}R_\lambda{}^{-1}]^{-1}. \tag{6.1}$$

If the viscous contribution (second term in brackets) and the non-local contributions (last term) are neglected, we recover the K41 spectrum with $c_1 = C_K$.

We should stress that all three contributions will be important only in the neighbourhood of Ψ_p. It is possible to choose the constants c_1, c_2 and c_3 to obtain a scaling consistent with the DNS data. In particular, the choice of $c_1 \approx 1.58$, $c_2 \approx 2$ and $c_3 \approx 2$ results in a Ψ_p that is close to the power law $R_\lambda{}^{-\gamma}$ found in figure 3.

Although a functional form for the entire spectrum is not known, the results in §§ 2 and 3 allow us to constrain the allowable form of (2.1). Figures 2 and 3 show that while Ψ_p decreases with Reynolds number, its location $k_p\eta$ as well as the height of the spectral dip Ψ_d and its location $k_d\eta$ are independent of the Reynolds number. Thus, the key spectral features of the dissipative range scale with Kolmogorov scales except for the amplitude of the bump, which contains a Reynolds number dependence. Since the inertial range scaling remains essentially independent of R_λ, it follows that a function of the form

$$\frac{E(k)}{u_\eta^2\eta} = g_1(k\eta)[1 + g_2(k\eta)h(R_\lambda)], \tag{6.2}$$

where $g_1(k\eta)$ characterizes the behaviour in the inertial and far-dissipation range, appears appropriate. The function g_1 is often represented as $g_1(k\eta) = C_K(k\eta)^{-5/3}\exp(-\alpha_1(k\eta)^{\alpha_2})$, where α_1 and α_2 are constants. The function $g_2(k\eta)$, on the other hand, characterizes the shape of the bump ($g(k\eta) \to 0$ as $k\eta \to 0$); its Reynolds number dependence is represented by $h(R_\lambda)$ which, as we have seen, can be approximated by $R_\lambda{}^{-\gamma}$. This suggests that some dependence on R_λ might remain in the far dissipation range (as is also clear for the model in figure 9*b*). This dependence, which may be ascribed to variations in α_1 and α_2, can also be due to residual effects of $h(R_\lambda)$ at higher wavenumbers. A precise answer requires a more systematic study.

7. Conclusions

Using data from DNS from several boxes up to 4096^3 grid size, covering Taylor microscale Reynolds numbers from 38 up to $\approx$1000, we investigated the scaling of the bottleneck effect and the difficulties it causes in the determination of the Kolmogorov constant C_K. We proposed an unambiguous way of determining the constant and showed that the result does not depend on data fitting ranges, particular power-law behaviour or intermittency corrections. The constant so determined is 1.58 for the three-dimensional spectrum, independent of R_λ.

The spectral bump decreases slowly with R_λ and may become negligible only for microscale Reynolds numbers greater than $O(10^5)$. This observation forces us to include a Reynolds number dependence even for small scales (i.e. (2.1)). Structure functions also possess Reynolds number effects in the transition between analytical and singular ranges. The DNS data suggest that the sharpness of this transition is related to the bottleneck in wavenumber space: a smoother transition means a diminished spectral bump.

Finally, we proposed a modified version of the widely used Batchelor formula (4.1) for second-order structure functions to take into account the Reynolds number dependence. By using (4.1) and a model for large scales, we have shown that large-scale

features of structure functions may appear at dissipative scales in wavenumber space. This result complicates the correspondence $r \sim 1/k$ usually used for phenomenological estimates. A simple model that takes into account local, non-local and viscous contributions has been proposed to reproduce the behaviour in the neighbourhood of the bottleneck. We note, however, that detailed studies of triadic interactions and their scaling with Reynolds numbers should be conducted to fully unveil the effect of non-local transfer.

Two directions naturally follow from this paper. First, simulations or experiments at higher R_λ that can reliably measure the three-dimensional spectrum are needed to address the asymptotic behaviour of both Ψ_d and Ψ_p. Second, it is necessary to investigate the far-dissipation region more systematically to determine the Reynolds number effects. Both issues are important in understanding the limitations of universality at finite Reynolds numbers. This is part of the ongoing research.

A final comment appears useful. Since the large-scale effects depend on the flow, some characteristics of the bottleneck can be expected to depend on the flow as well. Fortunately, at the present level of detail, the effect appears entirely through the large-scale L. Thus, we may expect some universality of the conclusions reached here.

The DNS database used in this work, including the data from the largest 4096^3 simulations, has been generated in collaboration with P. K. Yeung at the Georgia Institute of Technology. The authors would like to thank U. Frisch for useful comments on the ideas presented here. They also acknowledge the computational time at the Texas Advanced Computing Center, Austin, TX, and the National Institute for Computational Sciences, Oak Ridge, TN. This work was supported by the National Science Foundation Grants CBET-553867 and CTS-0553602.

REFERENCES

Aivalis, K. G., Sreenivasan, K. R., Tsuji, Y., Klewicki, J. C. & Biltoft, C. A. 2002 Temperature structure functions for air flow over moderately heated ground. *Phys. Fluids* **14**, 2439–2446.

Aoyama, T., Ishihara, T., Kaneda, Y., Yokokawa, M., Itakura, K. & Un, A. 2005 Statistics of energy transfer in high-resolution direct numerical simulation of turbulence in a periodic box. *J. Phys. Soc. Japan* **74**, 3202–3212.

Bailey, S. C. C., Hultmark, M., Schumacher, J., Yakhot, V. & Smits, A. J. 2009 Measurement of local dissipation scales in turbulent pipe flow. *Phys. Rev. Lett.* **103**, 014502.

Barenblatt, G. I. & Goldenfeld, N. 1995 Does fully developed turbulence exist? Reynolds number independence versus asymptotic covariance. *Phys. Fluids* **7**, 3078–3082.

Batchelor, G. K. 1951 Pressure fluctuations in isotropic turbulence. *Math. Proc. Camb. Phil. Soc.* **47**, 359–374.

Benzi, R., Ciliberto, S., Baudet, C., Chavarria, G. R. & Tripiccione, R. 1993 Extended self-similarity in the dissipation range of fully-developed turbulence. *Europhys. Lett.* **24** (4), 275–279.

Bershadskii, A. 2008 Near-dissipation range in nonlocal turbulence. *Phys. Fluids* **20** (8), 085103.

Cerutti, S. & Meneveau, C. 2000 Statistics of filtered velocity in grid and wake turbulence. *Phys. Fluids* **12** (5), 1143–1165.

Chen, S. Y., Dhruva, B., Kurien, S., Sreenivasan, K. R. & Taylor, M. A. 2005 Anomalous scaling of low-order structure functions of turbulent velocity. *J. Fluid Mech.* **533**, 183–192.

Chevillard, L., Castaing, B., Leveque, E. & Arneodo, A. 2006 Unified multifractal description of velocity increments statistics in turbulence: intermittency and skewness. *Physica* D **218** (1), 77–82.

Dhruva, B., Tsuji, Y. & Sreenivasan, K. R. 1997 Transverse structure functions in high-Reynolds-number turbulence. *Phys. Rev.* E **56** (5), R4928–R4930.

Dobler, W., Haugen, N. E. L., Yousef, T. A. & Brandenburg, A. 2003 Bottleneck effect in three-dimensional turbulence simulations. *Phys. Rev.* E **68** (2), 026304.

Donzis, D. A., Sreenivasan, K. R. & Yeung, P. K. 2005 Scalar dissipation rate and dissipative anomaly in isotropic turbulence. *J. Fluid Mech.* **532**, 199–216.

Donzis, D. A. & Yeung, P. K. 2009 Resolution effects and scaling in numerical simulations of passive scalar mixing in turbulence. *Physica* D, doi:10.1016/j.physd.2009.09.024.

Donzis, D. A., Yeung, P. K. & Pekurovsky, D. 2008*a* Turbulence simulations on $O(10^4)$ processors. In *TeraGrid 2008 Conference*, Las Vegas, NV, 9–13 June.

Donzis, D. A., Yeung, P. K. & Sreenivasan, K. R. 2008*b* Dissipation and enstrophy in isotropic turbulence: scaling and resolution effects in direct numerical simulations. *Phys. Fluids* **20**, 045108.

Eswaran, V. & Pope, S. B. 1988 An examination of forcing in direct numerical simulations of turbulence. *Comput. Fluids* **16**, 257–278.

Falkovich, G. 1994 Bottleneck phenomenon in developed turbulence. *Phys. Fluids* **6**, 1411–1414.

Frisch, U., Kurien, S., Pandit, R., Pauls, W., Ray, S. S., Wirth, A. & Zhu, J.-Z. 2008 Hyperviscosity, Galerkin truncation, and bottlenecks in turbulence. *Phys. Rev. Lett.* **101** (14), 144501.

Gotoh, G., Fukayama, D. & Nakano, T. 2002 Velocity field statistics in homogeneous steady turbulence obtained using a high-resolution direct numerical simulation. *Phys. Fluids* **14** (3), 1065–1081.

Kaimal, J. C., Izumi, Y., Wyngaard, J. C. & Cote, R. 1972 Spectral characteristics of surface-layer turbulence. *Q. J. R. Meteorol. Soc.* **417**, 563–589.

Kaneda, Y., Ishihara, T., Yokokawa, M., Itakura, K. & Uno, A. 2003 Energy dissipation rate and energy spectrum in high resolution direct numerical simulations of turbulence in a periodic box. *Phys. Fluids* **15** (2), L21–L24.

Kang, H. S., Chester, S. & Meneveau, C. 2003 Decaying turbulence in an active-grid-generated flow and comparisons with large-eddy simulation. *J. Fluid Mech.* **480**, 129–160.

Kolmogorov, A. N. 1941 Local structure of turbulence in an incompressible fluid for very large Reynolds numbers. *Dokl. Akad. Nauk. SSSR* **30**, 299–303.

Kurien, S., Taylor, M. A. & Matsumoto, T. 2004 Cascade time scales for energy and helicity in homogeneous isotropic turbulence. *Phys. Rev.* E **69** (6), 066313.

Lohse, D. 1994 Crossover from high to low-Reynolds-number turbulence. *Phys. Rev. Lett.* **73** (24), 3223–3226.

Lohse, D. & Müller-Groeling, A. 1995 Bottleneck effects in turbulence-scaling phenomena in r-space versus p-space. *Phys. Rev. Lett.* **74** (10), 1747–1750.

Lohse, D. & Müller-Groeling, A. 1996 Anisotropy and scaling corrections in turbulence. *Phys. Rev.* E **54** (1), 395–405.

Martinez, D. O., Chen, S., Doolen, G. D., Kraichnan, R. H., Wang, L. P. & Zhou, Y. 1997 Energy spectrum in the dissipation range of fluid turbulence. *J. Plasma Phys.* **57**, 195–201.

Meneveau, C. 1996 Transition between viscous and inertial-range scaling of turbulence structure functions. *Phys. Rev.* E **54** (4), 3657–3663.

Meyers, J. & Meneveau, C. 2008 A functional form for the energy spectrum parametrizing bottleneck and intermittency effects. *Phys. Fluids* **20** (6), 065109.

Mininni, P. D., Alexakis, A. & Pouquet, A. 2008 Nonlocal interactions in hydrodynamic turbulence at high Reynolds numbers: the slow emergence of scaling laws. *Phys. Rev.* E **77**, 036306.

Monin, A. S. & Yaglom, A. M. 1975 *Statistical Fluid Mechanics*, vol. 2. MIT Press.

Mydlarski, L. & Warhaft, Z. 1998 Passive scalar statistics in high-Peclet-number grid turbulence. *J. Fluid Mech.* **358**, 135–175.

Nelkin, M. 1990 Multifractal scaling of velocity derivatives in turbulence. *Phys. Rev.* A **42**, 7226–7229.

Obukhov, A. M. 1941 On the distribution of energy in the spectrum of turbulent flow. *Dokl. Akad. Nauk. SSSR* **32**, 22–24.

Praskovsky, A. & Oncley, S. 1994 Measurements of the Kolmogorov constant and intermittency exponent at very high Reynolds numbers. *Phys. Fluids* **6** (9), 2886–2888.

Praskovsky, A. & Oncley, S. 1997 Comprehensive measurements of the intermittency exponent in high Reynolds number turbulent flows. *Fluid Dyn. Res.* **21** (5), 331–358.

Qian, J. 1984 Universal equilibrium range of turbulence. *Phys. Fluids* **27**, 2229–2233.

She, Z.-S. & Jackson, E. 1993 On the universal form of energy spectra in fully developed turbulence. *Phys. Fluids* **5**, 1526–1528.

Sirovich, L., Smith, L. & Yakhot, V. 1994 Energy-spectrum of homogeneous and isotropic turbulence in far dissipation range. *Phys. Rev. Lett.* **72** (3), 344–347.

Sreenivasan, K. R. 1995 On the universality of the Kolmogorov constant. *Phys. Fluids* **7** (11), 2778–2784.

Sreenivasan, K. R. & Dhruva, B. 1998 Is there scaling in high-Reynolds-number turbulence? *Prog. Theor. Phys. Suppl.* **130**, 103–120.

Sreenivasan, K. R. & Kailasnath, P. 1993 An update on the intermittency exponent in turbulence. *Phys. Fluids* **5** (2), 512–514.

Stolovitzky, G., Sreenivasan, K. R. & Juneja, A. 1993 Scaling functions and scaling exponents in turbulence. *Phys. Rev.* E **48** (5), R3217–R3220.

Tsuji, Y. 2004 Intermittency effect on energy spectrum in high-Reynolds number turbulence. *Phys. Fluids* **16** (5), L43–L46.

Verma, M. K. & Donzis, D. A. 2007 Energy transfer and bottleneck effect in turbulence. *J. Phys.* A **40** (16), 4401–4412.

Watanabe, T. & Gotoh, T. 2007 Inertial-range intermittency and accuracy of direct numerical simulation for turbulence and passive scalar turbulence. *J. Fluid Mech.* **590**, 117–146.

Welter, G. S., Wittwer, A. R., Degrazia, G. A., Acevedo, O. C., Leal de Moraes, O. L. & Anfossi, D. 2009 Measurements of the Kolmogorov constant from laboratory and geophysical wind data. *Physica* A **388** (18), 3745–3751.

Yakhot, V. & Sreenivasan, K. R. 2005 Anomalous scaling of structure functions and dynamic constraints on turbulence simulations. *J. Stat. Phys.* **121**, 823–841.

Yakhot, V. & Zakharov, V. 1993 Hidden conservation-laws in hydrodynamics energy and dissipation rate fluctuation spectra in strong turbulence. *Physica* D **64** (4), 379–394.

Yeung, P. K. & Zhou, Y. 1997 Universality of the Kolmogorov constant in numerical simulations of turbulence. *Phys. Rev.* E **56**, 1746–1752.